

Veiled Talbot Effect

Murat Yessenov,^{1,*} Layton A. Hall^{1,*}, Sergey A. Ponomarenko,^{2,3} and Ayman F. Abouraddy¹

¹CREOL, The College of Optics and Photonics, University of Central Florida, Orlando, Florida 32816, USA

²Department of Electrical and Computer Engineering, Dalhousie University, Halifax, Nova Scotia B3J 2X4, Canada

³Department of Physics and Atmospheric Science, Dalhousie University, Halifax, Nova Scotia B3H 4R2, Canada



(Received 26 May 2020; accepted 13 November 2020; published 10 December 2020)

A freely propagating optical field having a periodic transverse spatial profile undergoes periodic axial revivals—a well-known phenomenon known as the Talbot effect or self-imaging. We show here that introducing tight spatiotemporal spectral correlations into an ultrafast pulsed optical field with a periodic transverse spatial profile eliminates all axial dynamics in physical space, while revealing a novel veiled Talbot effect that can be observed only when carrying out time-resolved measurements. Indeed, “time diffraction” is observed, whereupon the temporal profile of the field envelope at a fixed axial plane corresponds to a segment of the spatial propagation profile of a monochromatic field sharing the initial spatial profile and observed at the same axial plane. Time averaging, which is intrinsic to observing the intensity, altogether veils this effect.

DOI: [10.1103/PhysRevLett.125.243901](https://doi.org/10.1103/PhysRevLett.125.243901)

The long-known Talbot effect [1,2], or self-imaging [3], refers to a freely propagating paraxial optical field (at a wavelength λ_o) having a periodic transverse spatial profile (of period L) undergoing *periodic* axial revivals (at planes separated by the Talbot distance $z_T = 2L^2/\lambda_o$). The field evolution unique to the Talbot effect can be readily observed in physical space. Space-time duality [4] suggests that an analogous temporal Talbot effect [5–7] occurs when a periodic train of pulses (of period T) travels in a dispersive medium (with dispersion parameter k_2): the pulses initially disperse but are subsequently reconstituted axially at multiples of $z_T = T^2/\pi|k_2|$. This temporal evolution can be observed by a sufficiently fast detector. The Talbot effect has been used in a wide span of applications [8] extending most recently from structured illumination in fluorescence microscopy [9] to temporal cloaking [10] and prime-number decomposition [11].

An implicit—yet fundamental—assumption underlying the Talbot effect is the separability of the spatial and temporal degrees of freedom of the optical field. Imposing a periodic profile in either space or time implies discretizing the corresponding spectrum at multiples of $2\pi/L$ or $2\pi/T$, respectively, which raises a question with regard to the Talbot effect for pulsed optical fields in which the spatial and temporal degrees of freedom are inextricably intertwined. Specifically, the spectral support domain of so-called space-time (ST) wave packets tightly associates each *spatial* frequency with a single *temporal* frequency (or wavelength) [12–14], such that discretization of one degree of freedom inescapably entails discretization of the other. To date, such pulsed beams [15–17] have been synthesized exclusively with continuous spectra tailored to render them propagation invariant [18–20]. Indeed, it is now well

established that they are transported rigidly in free space at a fixed, but arbitrary group velocity [21–24]. Self-imaging of ST wave packets lacking themselves a periodic structure (thus retaining a continuous spectrum) was examined theoretically by superposing wave packets of different phase velocities [25] and realized in space by superposing pulsed Bessel beams [26] (self-imaging in both cases is thus unrelated to the Talbot effect).

We pose here a question regarding the propagation of ST wave packets having periodic transverse spatial profiles, whereupon the spatial *and* temporal spectra are simultaneously discretized on account of their tight association. Two mutually exclusive scenarios appear to be on offer. If the spatiotemporal structure undergirding propagation invariance plays the same role with discrete spectra as with continuous spectra, then any axial dynamics will be arrested and self-imaging thwarted. Alternatively, spatiotemporal spectral discretization may disrupt the propagation invariance of periodic ST wave packets and lead to self-imaging at the Talbot planes.

Here we show that aspects of both contradictory scenarios are realized by ST wave packets when endowed with a periodic spatial profile, leading to a remarkable phenomenon: a *veiled* Talbot effect. We find that no spatial axial dynamics is discernible in the time-averaged intensity, and no axial temporal dynamics is discernible in the space-averaged intensity; Talbot revivals are altogether absent. This points to the impact of the unique spectral structure of ST wave packets trumping that of spectral discretization, whereby the initial periodic spatial profile propagates self-similarly and may even, in fact, display no spatial features whatsoever. Nevertheless, time-resolved measurements of the spatial profile unveil spectral-discretization-induced

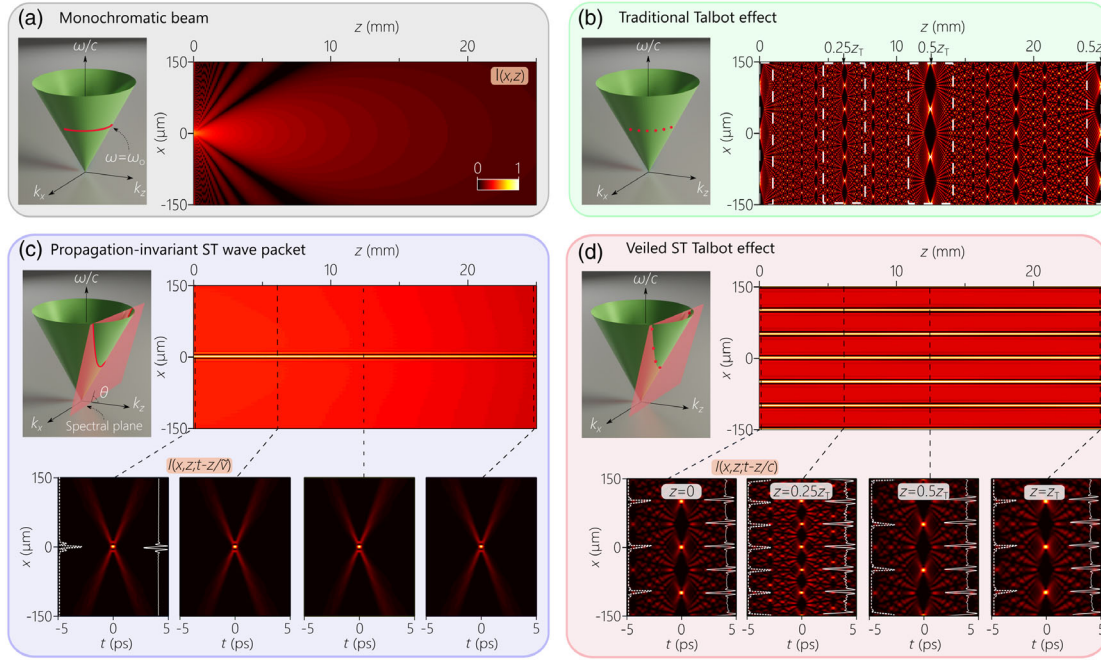


FIG. 1. Concept of the veiled Talbot effect. (a) The axial evolution of the intensity $I(x, z)$ for a monochromatic ($\lambda_o = 800$ nm) plane wave illuminating an aperture of width $\Delta x = 10 \mu\text{m}$. On the left we depict the light cone $k_x^2 + k_z^2 = (\omega/c)^2$ and the field spectral support domain on its surface. (b) Plot of $I(x, z)$ for a monochromatic field $\lambda_o = 800$ nm with periodic transverse spatial profile of period $L = 100$ and $\Delta x = 10 \mu\text{m}$, exhibiting the traditional Talbot effect with $z_T = 25$ mm. (c) The intensity $I(x, z)$ for a ST wave packet with $\lambda_o = 800$ nm, $\Delta\lambda = 2$ nm, $\Delta x = 10 \mu\text{m}$, and $\theta = 80^\circ$. The lower panels are the invariant spatiotemporal profiles $I(x, z; t)$ in a frame moving at \tilde{v} at selected axial planes. (d) Same as (c) except that the spatial spectrum is sampled at integer multiples of $2\pi/L$, with $L = 100 \mu\text{m}$; $I(x, z)$ has a transverse period of $L/2 = 50 \mu\text{m}$ rather than $100 \mu\text{m}$, and there are no discernible axial changes. The lower panels are $I(x, z; t)$ in a frame moving at c at selected axial planes, thereby revealing veiled periodic Talbot revivals. In each panel, the white dashed curve on the left is the spatial profile at $t = 0$, which evolves along z and is periodic with period L at $z = mz_T$, whereas the white curve on the right is the time-averaged intensity $I(x, z)$, which is independent of z and is periodic with period $L/2$.

axial dynamics that disrupts propagation invariance: the temporal dynamics at every axial plane recapitulates a different portion of the spatial dynamics of the traditional Talbot effect, which can be shown to be a new manifestation of time diffraction [27–30]. Revivals occur at the Talbot planes with complex axial dynamics enfolded in intervening planes, which is veiled from view in physical space. Moreover, we encounter an unanticipated effect: the disparity of the *transverse* period observed in space from that observed in space-time. Although the spatial spectrum is sampled at multiples of $2\pi/L$, the observed period in space is nevertheless $L/2$, rather than the expected value L that is observed in space-time. These phenomena associated with the veiled Talbot effect indicate more generally the rich repertoire of behavior intrinsic to fields endowed with precise spatiotemporal structures.

We first outline the theoretical basis for the veiled Talbot effect (see Supplemental Material [31]). Throughout, we consider for simplicity optical fields propagating along z that are uniform over the transverse coordinate y (i.e., a light sheet modulated along the transverse coordinate x). A monochromatic paraxial field at a fixed temporal (angular) frequency $\omega = \omega_o$ and wave number $k_o = \omega_o/c$

diffraction along z [Fig. 1(a)]. Writing the field as $E(x, z; t) = e^{i(k_o z - \omega_o t)} \psi_x(x, z)$, the envelope is given by $\psi_x(x, z) = \int dk_x \tilde{\psi}(k_x) \exp\{i(k_x x - (k_x^2/2k_o)z)\}$, where k_x is the transverse component of the wave vector (denoted the spatial frequency), and the spatial spectrum $\tilde{\psi}(k_x)$ is the Fourier transform of $\psi_x(x, 0)$. If the transverse field is periodic with period L , the spatial spectrum is discretized $k_x \rightarrow nk_L$, $\tilde{\psi}(k_x) \rightarrow \tilde{\psi}(nk_L) = \tilde{\psi}_n$, and $\psi_x(x, z) = \sum_n \tilde{\psi}_n \exp\{i2\pi n(x/L - n(z/z_T))\}$; n is an integer and $k_L = 2\pi/L$. Consequently, the initial profile is revived periodically at the Talbot planes $\psi_x(x, mz_T) = \psi_x(x, 0)$ for integer m , with rich and striking dynamics enfolded between these planes [Fig. 1(b)]. Similar dynamics is observed when *pulsed* fields are employed in which the spatial and temporal degrees of freedom are separable—as in most mode-locked lasers, which allows k_x to be discretized while maintaining $\Omega = \omega - \omega_o$ continuous.

However, other pulsed-beam configurations have been recently explored in which the spatial and temporal degrees of freedom are nonseparable, leading to novel emergent behaviors, including propagation invariance [18,19], controllable group velocities [20–24,35–37], transverse orbital angular momentum [38], ultrafast beam steering [39], and

omniresonant interactions with planar cavities [40,41]. We consider here ST wave packets satisfying the spectral condition $\Omega = (k_z - k_o)c \tan \theta$, which represents a plane in $(k_x, k_z, \omega/c)$ space that makes an angle θ (the spectral tilt angle) with respect to the k_z axis [14]. The constraint $k_x^2 + k_z^2 = (\omega/c)^2$ imposes a relationship between the spatial and temporal frequencies in the paraxial regime $\Omega/c(1 - \cot \theta) = k_x^2/2k_o$, leading to a propagation-invariant (diffraction-free and dispersion-free) envelope,

$$\begin{aligned} \psi(x, z; t) &= \int dk_x \tilde{\psi}(k_x) e^{ik_x x} e^{-i\Omega(t-z/\tilde{v})} \\ &= \psi(x, 0; t - z/\tilde{v}), \end{aligned} \quad (1)$$

representing a wave packet traveling rigidly at a group velocity $\tilde{v} = c \tan \theta$ that can be tuned by changing θ , and $\tilde{\psi}(k_x)$ is the Fourier transform of $\psi(x, 0, 0)$. The time-averaged intensity $I(x, z) = \int dt |\psi(x, z; t)|^2 = \int dk_x |\tilde{\psi}(k_x)|^2 + \text{Re} \int dk_x \tilde{\psi}(k_x) \tilde{\psi}^*(-k_x) e^{i2k_x x}$ as recorded by a slow detector (e.g., a camera) is independent of z [Fig. 1(c)]. The factor of 2 in the exponent of the second term indicates that $I(x, z)$ is scaled spatially by a factor of 2 with respect to the time-resolved intensity profile $I(x, z; t) = |\psi(x, z; t)|^2$, a point we will return to shortly. Finally, the unavoidable uncertainty in the association between spatial and temporal frequencies limits the temporal window over which the ST wave packet can be observed [42].

When the transverse spatial profile is periodic and the spatial spectrum discretized $k_x \rightarrow nk_L$, the tight association between spatial and temporal frequencies entails that the temporal frequencies are *also* discretized $\Omega \rightarrow n^2\Omega_L$, $\Omega_L = 2\pi/z_T(c/|1 - \cot \theta|)$, and the envelope becomes

$$\psi(x, z; t) = \sum_{n=-\infty}^{\infty} \tilde{\psi}_n e^{i2\pi n \frac{x}{L}} e^{-i2\pi n^2 \frac{z}{z_T}} e^{i\frac{2\pi n^2(z-ct)}{z_T(1-\cot \theta)}}. \quad (2)$$

Therefore, $\psi(x, mz_T; t - mz_T/c) = \psi(x, 0; t)$; that is, at the Talbot planes in a reference frame propagating at $\tilde{v} = c$, the initial field distribution at $z = 0$ is retrieved. Furthermore, comparing the formulas for the monochromatic field and the ST wave packet, we find that $\psi(x, z; t - z/c) = \psi_x(x, z + ct/1 - \cot \theta)$. In other words, the time-resolved spatial distribution of a ST wave packet at a fixed plane z corresponds to the axial spatial distribution of a *monochromatic* periodic field after replacing axial displacement with a scaled time variable, which is a manifestation of time diffraction [27–30]; see Fig. 1(d). The time-averaged intensity $I(x, z)$ is

$$I(x, z) = \sum_n |\tilde{\psi}_n|^2 + \sum_n \tilde{\psi}_n \tilde{\psi}_{-n}^* e^{i2 \times 2\pi \frac{x}{L}}, \quad (3)$$

which does not include z and thus indicates the complete absence of axial dynamics. It can be shown [43] that a

one-to-one association between spatial and temporal frequencies—which is maintained here after spectral discretization—is a sufficient condition for a diffraction-free time-averaged intensity $I(x, z) \rightarrow I(x)$. Furthermore, the spatial frequency has doubled (corresponding to half the transverse spacing), so we expect a period of $L/2$ in $I(x, z)$ in contrast to a period L in $I(x, z; t)$, in addition to a scaling in the size of the features in each period [Fig. 1(d)].

We have carried out experiments to confirm this predicted veiled Talbot effect by utilizing the two-dimensional pulse shaper developed in Refs. [19,22,23] to synthesize superluminal ST wave packets at a spectral tilt angle of $\theta = 80^\circ$ ($\tilde{v} \approx 5.67c$), starting with femtosecond pulses from a Ti:sapphire laser (see Supplemental Material [31]). Using a spatial light modulator, we sample the spatial spectrum at nk_L and concurrently sample the temporal spectrum at $n^2\Omega_L$ over a temporal bandwidth of $\Delta\lambda \approx 2$ nm, corresponding to temporal features of width $\Delta\tau \sim 2.5$ ps and spatial features of width $\Delta x \sim 25$ μm in the spatiotemporal profile. We measure $I(x, z)$ by scanning a CCD camera along z , the spatiotemporal spectrum, and $I(x, z; \tau)$ measured interferometrically at different axial planes in a reference frame moving at a group velocity of c .

We first sample the spatial spectrum at multiples of $2\pi/L$ with $L = 80$ μm [Fig. 2(a)]. Nevertheless, the measured intensity [Fig. 2(a)] shows a periodic transverse profile of period $L/2 = 40$ μm rather than $L = 80$ μm , and no trace of the Talbot effect is observable. Indeed, the axial propagation is invariant just as in previous studies of ST wave packets having continuous spectra. However, time-resolved measurements reveal a different picture altogether. The dynamics in the measured spatiotemporal profiles $I(x, z; \tau)$ acquired in a reference frame moving at c [Fig. 2(b)] is completely veiled in the time-averaged measurements [Fig. 2(a)]. We note the revivals at $z = z_T$ and $2z_T$ and those at $z = 0.5z_T$, $1.5z_T$, and $2.5z_T$, all with a transverse period of $L = 80$ μm . The patterns are shifted along x by $L/2$ midway between the Talbot planes, whereupon the “dark” and “bright” features are exchanged with respect to those in the Talbot planes. In contrast, if the spectrum remains continuous without sampling, both the intensity $I(x, z)$ and the spatiotemporal profile $I(x, z; \tau)$ lack periodicity and are invariant at *all* axial planes (Supplemental Material [31]).

To resolve the dynamics within a single Talbot length, we increase the period to $L = 160$ μm ($z_T = 64$ mm) by increasing the spectral sampling rate. The measured intensity $I(x, z)$ [Fig. 2(c)] remains invariant with z , shows no axial dynamics, and has a transverse period $L/2 = 80$ μm rather than $L = 160$ μm . The spatiotemporal profiles of the ST wave packet measured at 5 planes within a Talbot length at $z = 0.15z_T$, $0.25z_T$, $0.35z_T$, $0.5z_T$, and $0.65z_T$ reveal complex dynamics in which energy is exchanged between the peaks in the profile [Fig. 2(d)]. At $z = 0.5z_T$ the transverse period is $L = 160$ μm , and at $z = 0.25z_T$ is

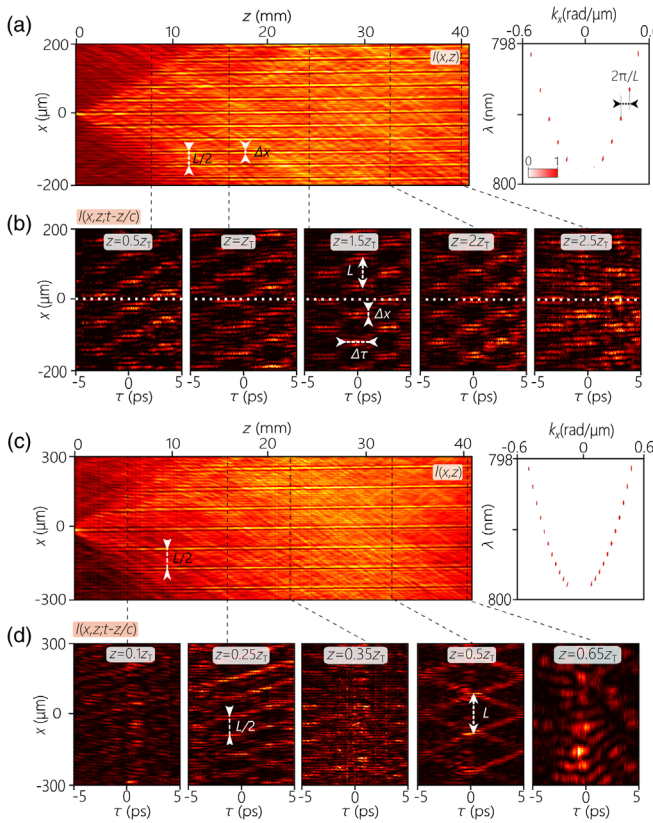


FIG. 2. Measurements of veiled Talbot revivals. (a) The measured $I(x, z)$ for a ST wave packet whose spatial spectrum is sampled at multiples of $2\pi/L$ (shown on the right); $L = 80 \mu\text{m}$, $z_T = 16 \text{ mm}$, $\theta = 80^\circ$, $\lambda_o \approx 799.1 \text{ nm}$, $\Delta\lambda = 2 \text{ nm}$, and $\Delta x = 10 \mu\text{m}$. The transverse period is $L/2 = 40 \mu\text{m}$, and no axial dynamics is discernible. (b) Measured $I(x, z; \tau)$ at $z = 0.5z_T, z_T, 1.5z_T, 2z_T$, and $2.5z_T$. The transverse period is $L = 80 \mu\text{m}$, $\Delta x \approx 20\text{--}30 \mu\text{m}$, and $\Delta\tau \approx 2.5 \text{ ps}$. The white dotted line is a guide for the eye at $x = 0$. (c) Same as (a) but with $L = 160 \mu\text{m}$ ($z_T = 64 \mu\text{m}$). The observed transverse period is $L/2 = 80 \mu\text{m}$. (d) Measured $I(x, z; \tau)$ at $z = 0.1z_T, 0.25z_T, 0.35z_T, 0.5z_T$, and $0.65z_T$; $\Delta x \approx 25\text{--}30 \mu\text{m}$, $\Delta\tau \approx 2.5\text{--}3 \text{ ps}$, and the measured transverse period is $L = 160 \text{ mm}$ at $z = 0.5z_T$.

$L/2 = 80 \mu\text{m}$, albeit with less contrast in comparison to the Talbot planes. At intermediate planes, the spatiotemporal profile takes on quasirandom distributions before returning to more recognizable profiles at Talbot half and quarter lengths. Once again, this dynamics is fully hidden from view in the spatial intensity [Fig. 2(c)]. These experimental observations are all in excellent agreement with simulations of ST wave packets after discretizing the spatiotemporal spectrum (Supplemental Material [31], Videos 1 and 2).

The factor of 2 in the time-averaged intensity [Eq. (3)] with respect to spatiotemporal envelope [Eq. (2)] appears regularly in correlation functions in the context of optical coherence after averaging over a statistical ensemble. However, the underlying stochastic fields are inaccessible, and the correlation functions are the only observables. Here, we capture the intensity after time averaging (which

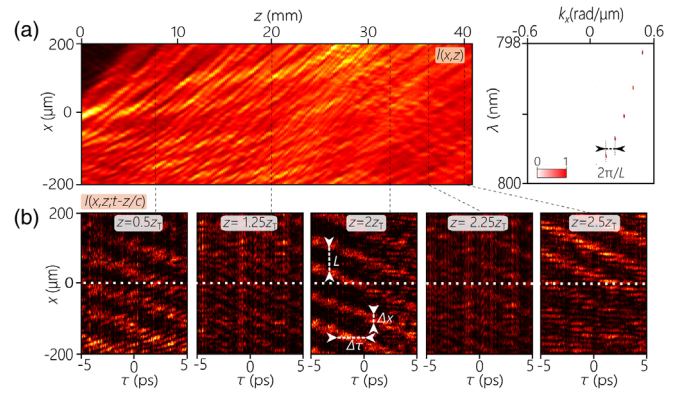


FIG. 3. Measurements of veiled Talbot revivals for a one-sided spatial spectrum. (a) The measured intensity $I(x, z)$ with the same parameters in Fig. 2(a) (except that only positive spatial frequencies are retained, shown on the right). There are no discernible transverse spatial features. (b) Measured spatiotemporal profiles at $z = 0.5z_T, 1.25z_T, 2z_T, 2.25z_T$, and $2.5z_T$, where $z_T = 16 \text{ mm}$, $\Delta x \approx 20\text{--}30 \mu\text{m}$, and $\Delta\tau \approx 2\text{--}3 \text{ ps}$.

is entangled with the spatial degree of freedom [13]) and the underlying spatiotemporal profile prior to time averaging, thus allowing an unambiguous observation of the impact of this spatial-scaling factor in changing the transverse period in the two distinct domains.

The veiled nature of the Talbot effect can be brought out even further by blocking half the spatial spectrum; $\tilde{\psi}_n = 0$ when $n < 0$. The intensity becomes a constant $I(x, z) = \sum_{n=0}^{\infty} |\tilde{\psi}_n|^2$ independent of x and z . Measurements of $I(x, z)$ are shown in Fig. 3(a) using the same parameters from Fig. 2(a) except for the one-sided spectrum. The spatiotemporal profiles measured at different axial planes reveal the underlying periodic transverse axial structure that is altogether veiled in the intensity and verify the axial dynamics associated with time diffraction. The Talbot effect is seen in the self-imaging revivals at $z = 1.25z_T$ and $2.25z_T$, and at $z = 0.5z_T$ and $2.5z_T$ (see Supplemental Material [31], Video 3).

The unique behaviors observed and recent advances achieved using ST wave packets rely on inculcating a precise spatiotemporal structure into the optical field. This Letter raises the question regarding which features of ST wave packets survive spectral discretization. We have shown that propagation invariance is maintained in the time-averaged intensity after spectral discretization. Note that the temporal spectrum is *not* discretized periodically, so there is no periodic pattern in time, and the field does not propagate in a dispersive medium, as required for exhibiting a temporal Talbot effect. Instead, the underlying field undergoes periodic revivals at the planes defined by the spatial Talbot length, signifying that the complex dynamics observed in the measured time-resolved self-imaging Talbot revivals are a manifestation of time diffraction, all of which is completely veiled in the spatial intensity profile. Although we have couched this phenomenon in terms of

optical fields, it is applicable to any other waves, such as acoustics or matter waves. We believe these findings have potential applications in the field of transient absorption spectroscopy, multiphoton lithography [44], and temporal imaging [45].

This work was funded by the U.S. Office of Naval Research (ONR) Contract No. N00014-17-1-2458 and ONR MURI Contract No. N00014-20-1-2789.

*These authors contributed equally to this work.

- [1] H. F. Talbot, Facts relating to optical science. No. IV, *Philos. Mag.* **9**, 401 (1836).
- [2] M. V. Berry and S. Klein, Integer, fractional and fractal Talbot effects, *J. Mod. Opt.* **43**, 2139 (1996).
- [3] W. D. Montgomery, Self-imaging objects of infinite aperture, *J. Opt. Soc. Am.* **57**, 772 (1967).
- [4] B. H. Kolner, Space-time duality and the theory of temporal imaging, *IEEE J. Quantum Electron.* **30**, 1951 (1994).
- [5] T. Jansson and J. Jansson, Temporal self-imaging effect in single-mode fibers, *J. Opt. Soc. Am.* **71**, 1373 (1981).
- [6] P. Andrekson, Linear propagation of optical picosecond pulse trains over oceanic distances, *Opt. Lett.* **18**, 1621 (1993).
- [7] F. Mitschke and U. Morgner, The temporal Talbot effect, *Opt. Photonics News* **9**, 45 (1998).
- [8] J. Wen, Y. Zhang, and M. Xiao, The Talbot effect: Recent advances in classical optics, nonlinear optics, and quantum optics, *Adv. Opt. Photonics* **5**, 83 (2013).
- [9] S. Chowdhury, J. Chen, and J. A. Izatt, Structured illumination fluorescence microscopy using Talbot self-imaging effect for high-throughput visualization, [arXiv:1801.03540](https://arxiv.org/abs/1801.03540).
- [10] B. Li, X. Wang, J. Kang, Y. Wei, T. Yung, and K. K. Y. Wong, Extended temporal cloak based on the inverse temporal Talbot effect, *Opt. Lett.* **42**, 767 (2017).
- [11] K. Pelka, J. Graf, T. Mehringer, and J. von Zanthier, Prime number decomposition using the Talbot effect, *Opt. Express* **26**, 15009 (2018).
- [12] R. Donnelly and R. Ziolkowski, Designing localized waves, *Proc. R. Soc. A* **440**, 541 (1993).
- [13] H. E. Kondakci, M. A. Alonso, and A. F. Abouraddy, Classical entanglement underpins the propagation invariance of space-time wave packets, *Opt. Lett.* **44**, 2645 (2019).
- [14] M. Yessenov, B. Bhaduri, H. E. Kondakci, and A. F. Abouraddy, Classification of propagation-invariant space-time light-sheets in free space: Theory and experiments, *Phys. Rev. A* **99**, 023856 (2019).
- [15] J. Turunen and A. T. Friberg, Propagation-invariant optical fields, *Prog. Opt.* **54**, 1 (2010).
- [16] *Non-Diffracting Waves*, edited by H. E. Hernández-Figueroa, E. Recami, and M. Zamboni-Rached (Wiley-VCH, New York, 2014).
- [17] M. A. Porras, Nature, diffraction-free propagation via space-time correlations, and nonlinear generation of time-diffracting light beams, *Phys. Rev. A* **97**, 063803 (2018).
- [18] P. Saari and K. Reivelt, Evidence of X-Shaped Propagation-Invariant Localized Light Waves, *Phys. Rev. Lett.* **79**, 4135 (1997).
- [19] H. E. Kondakci and A. F. Abouraddy, Diffraction-free space-time light sheets, *Nat. Photonics* **11**, 733 (2017).
- [20] L. J. Wong and I. Kaminer, Ultrashort tilted-pulsefront pulses and nonparaxial tilted-phase-front beams, *ACS Photonics* **4**, 2257 (2017).
- [21] J. Salo and M. M. Salomaa, Diffraction-free pulses at arbitrary speeds, *J. Opt. A* **3**, 366 (2001).
- [22] H. E. Kondakci and A. F. Abouraddy, Optical space-time wave packets of arbitrary group velocity in free space, *Nat. Commun.* **10**, 929 (2019).
- [23] B. Bhaduri, M. Yessenov, and A. F. Abouraddy, Space-time wave packets that travel in optical materials at the speed of light in vacuum, *Optica* **6**, 139 (2019).
- [24] B. Bhaduri, M. Yessenov, and A. F. Abouraddy, Anomalous refraction of optical spacetime wave packets, *Nat. Photonics* **14**, 416 (2020).
- [25] K. Reivelt, Self-imaging of three-dimensional images by pulsed wave fields, *Opt. Express* **10**, 360 (2002).
- [26] M. Bock, A. Treffer, and R. Grunwald, Nondiffracting self-imaging of ultrashort wavepackets, *Opt. Lett.* **42**, 2374 (2017).
- [27] M. Moshinsky, Diffraction in time, *Phys. Rev.* **88**, 625 (1952).
- [28] S. Longhi, Gaussian pulsed beams with arbitrary speed, *Opt. Express* **12**, 935 (2004).
- [29] M. A. Porras, Gaussian beams diffracting in time, *Opt. Lett.* **42**, 4679 (2017).
- [30] H. E. Kondakci and A. F. Abouraddy, Airy Wave Packets Accelerating in Space-Time, *Phys. Rev. Lett.* **120**, 163901 (2018).
- [31] See Supplemental Material at <http://link.aps.org/supplemental/10.1103/PhysRevLett.125.243901> for detailed theoretical analysis, a description of the measurement configuration and procedure, and theoretical predictions corresponding to the measurements presented here, which includes Refs. [32–34].
- [32] A. Sezginer, A general formulation of focus wave modes, *J. Appl. Phys.* **57**, 678 (1985).
- [33] M. Yessenov, B. Bhaduri, H. E. Kondakci, and A. F. Abouraddy, Weaving the rainbow: Space-time optical wave packets, *Opt. Photonics News* **30**, 34 (2019).
- [34] M. Yessenov, B. Bhaduri, P. J. Delfyett, and A. F. Abouraddy, Free-space optical delay line using space-time wave packets, *Nat. Commun.* **11**, 5782 (2020).
- [35] A. Sainte-Marie, O. Gobert, and F. Quéré, Controlling the velocity of ultrashort light pulses in vacuum through spatio-temporal couplings, *Optica* **4**, 1298 (2017).
- [36] D. H. Froula, D. Turnbull, A. S. Davies, T. J. Kessler, D. Haberberger, J. P. Palastro, S.-W. Bahk, I. A. Begishev, R. Boni, S. Bucht, J. Katz, and J. L. Shaw, Spatiotemporal control of laser intensity, *Nat. Photonics* **12**, 262 (2018).
- [37] S. W. Jolly, O. Gobert, A. Jeandet, and F. Quéré, Controlling the velocity of a femtosecond laser pulse using refractive lenses, *Opt. Express* **28**, 4888 (2020).
- [38] A. Chong, C. Wan, J. Chen, and Q. Zhan, Generation of spatiotemporal optical vortices with controllable transverse orbital angular momentum, *Nat. Photonics* **14**, 350 (2020).
- [39] A. M. Shaltout, K. G. Lagoudakis, J. van de Groep, S. J. Kim, J. Vučković, V. M. Shalaev, and M. L. Brongersma,

- Spatiotemporal light control with frequency-gradient metasurfaces, *Science* **365**, 374 (2019).
- [40] A. Shiri, M. Yessenov, R. Aravindakshan, and A. F. Abouraddy, Omni-resonant space-time wave packets, *Opt. Lett.* **45**, 1774 (2020).
- [41] A. Shiri, K. L. Schepler, and A. F. Abouraddy, Programmable omni-resonance using space-time fields, *APL Photonics* **5**, 106107 (2020).
- [42] M. Yessenov, B. Bhaduri, L. Mach, D. Mardani, H. E. Kondakci, M. A. Alonso, G. A. Atia, and A. F. Abouraddy, What is the maximum differential group delay achievable by a space-time wave packet in free space?, *Opt. Express* **27**, 12443 (2019).
- [43] M. Yessenov, B. Bhaduri, H. E. Kondakci, M. Meem, R. Menon, and A. F. Abouraddy, Diffraction-free broadband incoherent space-time fields, *Optica* **6**, 598 (2019).
- [44] S. Maruo and J. T. Fourkas, Recent progress in multiphoton microfabrication, *Laser Photonics Rev.* **2**, 100 (2008).
- [45] F. Shateri, M. H. Alizadeh, and Z. Kavehvasht, Temporal super resolution imaging inspired by structured illumination microscopy, *Opt. Commun.* **467**, 125742 (2020).